



This is the accepted manuscript made available via CHORUS. The article has been published as:

# Optical Frequency Metrology Study on Nonlinear Processes in a Waveguide Device for Ultrabroadband Comb Generation

Kazumichi Yoshii, Junia Nomura, Kaho Taguchi, Yusuke Hisai, and Feng-Lei Hong

Phys. Rev. Applied **11**, 054031 — Published 10 May 2019

DOI: [10.1103/PhysRevApplied.11.054031](https://doi.org/10.1103/PhysRevApplied.11.054031)

# Study on Nonlinear Processes in Waveguide Device for Ultra-Broadband Comb Generation Using Optical Frequency Metrology

Kazumichi Yoshii,<sup>1,2,\*</sup> Junia Nomura,<sup>1,2</sup> Kaho Taguchi,<sup>1</sup> Yusuke Hisai,<sup>1,2</sup> and Feng-Lei Hong<sup>1,2,†</sup>

<sup>1</sup>*Department of Physics, Graduate School of Engineering Science, Yokohama National University, 79-5 Tokiwadai, Hodogaya-ku, Yokohama 240-8501, Japan*

<sup>2</sup>*Japan Science and Technology Agency, ERATO MINOSHIMA Intelligent Optical Synthesizer Project, 1-5-1 Chofugaoka, Chofu, Tokyo 182-8585, Japan*

(Received )

We demonstrate an absolute frequency measurement using the ultra-broadband comb generated in a periodically poled lithium niobate waveguide (PPLN-WG). Based on the measured frequency information, we determine that the spectral broadening in the PPLN-WG is due to quadratic nonlinearity. We also show that the self-referenced carrier-envelope offset beat signal observed in the ultra-broadband comb is generated based on the  $2f-3f$  interference of different comb series. This study is not only useful for the practical application of frequency measurement but is also important for basic research of nonlinear optics.

## I. INTRODUCTION

Optical frequency combs (OFCs) have been demonstrated to be indispensable tools not only for precision frequency metrology [1,2], but also for use in fields including astronomy [3] and environmental monitoring [4]. An important characteristic of OFCs is their broad spectral coverage. The wide coverage of the comb spectrum is essential for the observation of the carrier-envelope offset (CEO) frequency [5] of an OFC and enables various applications within the comb spectrum range. The earlier stage OFC, using a mode-locked Ti:Sapphire laser, usually covers a spectral range of 500–1000 nm, while the currently popular OFC, using a mode-locked Er-doped fiber laser (Er: fiber comb), ranges from 1000–2000 nm. The rapid research progress of Er: fiber combs is mostly due to the reliability (continuous long-term operation) of the comb system.

To further broaden the comb spectrum for wider applications, various techniques of nonlinear optics must be used. For example, second harmonic generation (SHG) with a bulk periodically poled lithium niobate (PPLN) crystal is usually used for the generation of a visible comb from an Er: fiber comb for frequency measurement in the visible region. Furthermore, difference frequency generation (DFG) has been used to generate a mid-infrared comb from an Er: fiber comb [6,7]. In these techniques based on quadratic nonlinearity ( $\chi^{(2)}$ ), the obtained spectrum is usually limited within a relatively narrow bandwidth allowed by the phase-matching condition. A broadband comb covering more than 1 octave has been generated by coupling the SHG of an Er: fiber comb to a photonic crystal fiber (PCF) [8,9]. The

strong optical confinement inside the PCF results in spectral broadening through self-phase modulation based on a cubic nonlinearity ( $\chi^{(3)}$ ).

Recently, ultra-broadband combs covering up to 4 octaves have been generated in PPLN waveguides (PPLN-WGs) using not only Er-doped [10–13], but also Yb-doped [10] and Tm-doped [14] fiber lasers. The nonlinearity associated with the spectral broadening in these experiments was not self-evident. For example, the PPLN-WG used in [11] was designed for the generation of a mid-infrared (MIR) comb using near-infrared (NIR) combs based on DFG. Nevertheless, the generated comb covers a range of 0.35–4.4  $\mu\text{m}$ , including the MIR and visible spectral regions. Numerical simulations [13,14] of the structure of the broadened spectrum have provided evidence that shows the spectral broadening in PPLN-WGs is based on the cascaded- $\chi^{(2)}$  nonlinearity [15]. Meanwhile, a simulation has indicated that the spectral broadening in an aluminum nitride waveguide (AlN-WG) is mainly based on the  $\chi^{(3)}$  nonlinearity [16]. We believe that it is important to verify the nonlinear processes in such nonlinear media using not only the spectral structure information, but also the frequency information of individual comb lines.

Some experiments have already demonstrated that the generated supercontinuum in a nonlinear waveguide is a coherent comb [11,12,14,16]. Iwakuni et al. also demonstrated that the generated ultra-broadband comb can be used for the beat frequency measurement at 633 nm [11]. So far, an absolute frequency measurement has not been demonstrated using an ultra-broadened comb generated in a PPLN-WG.

In this article, we determine that the spectral broadening in a PPLN-WG is due to the  $\chi^{(2)}$  nonlinearity using the measured CEO frequency of an ultra-broadband comb. Based on the CEO frequency information, we also reveal that the self-referenced CEO beat signal observed in the

\*yoshii-kazumichi-mn@ynu.jp

†hong-fl@ynu.ac.jp

ultra-broadband comb is generated from the  $2f - 3f$  interference between different comb series. We also demonstrate the absolute frequency measurement of an iodine-stabilized Nd:YAG laser at 532 nm using the generated ultra-broadband comb. Furthermore, we discuss the spectral structure variation of the ultra-broadband comb based on higher order quasi phase matching (QPM) SHG due to the cascaded- $\chi^{(2)}$  process. The present experiment demonstrates an important application of precision frequency metrology in the research field of nonlinear optics. The absolute frequency measurement using the generated ultra-broadband comb shows an important example for the practical usage of the broadband comb.

## II. MEASUREMENT PRINCIPLE

In this section, we describe the method used to determine the nonlinear process involved in spectral broadening using optical frequency metrology. Figure 1 shows a schematic of the one-to-one correspondence between the nonlinear process and the CEO frequency of the broadened comb for two cases. *Case1*: The broadened comb is generated by the  $\chi^{(2)}$  process, namely SHG and sum-frequency generation (SFG). In this case, the CEO frequency of the original comb is  $f_{\text{CEO}}$  and the CEO frequency of the broadened comb is  $2f_{\text{CEO}}$ . We note that there is a possibility for the existence of another broadened comb series resulting from further SFG between the original comb and the firstly broadened comb. This comb series will have a CEO frequency of  $3f_{\text{CEO}}$ . *Case2*: The broadened comb

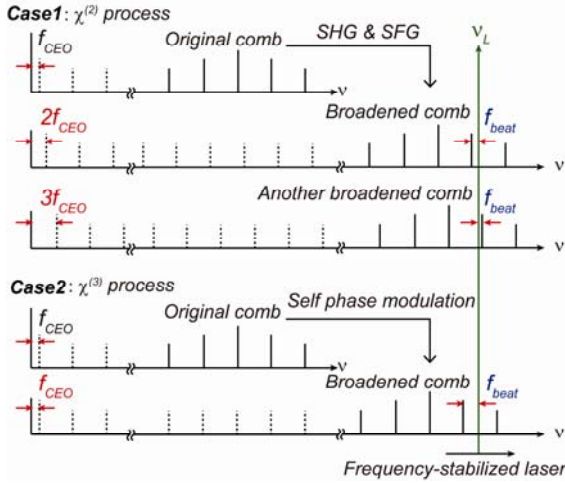


Fig. 1. Schematic of the one-to-one correspondence between the nonlinear process and the CEO frequency of the broadened comb. When the CEO frequency of the original comb is  $f_{\text{CEO}}$ , the CEO frequency of the broadened comb via the  $\chi^{(2)}$  process is  $2f_{\text{CEO}}$ . Meanwhile, the CEO frequency of the broadened comb via the  $\chi^{(3)}$  process is  $f_{\text{CEO}}$ .  $\nu_L$ , frequency of a frequency-stabilized laser;  $f_{\text{beat}}$ , beat frequency between the frequency-stabilized laser and the comb components; SHG, second-harmonic generation; SFG, sum-frequency generation.

is generated by the  $\chi^{(3)}$  process, namely self-phase modulation or four-wave mixing. In this case, the CEO frequency of the broadened comb is  $f_{\text{CEO}}$ , the same as the original comb.

In Fig. 1, we also illustrate the frequency relationships between a frequency-stabilized laser and the broadened combs.  $f_{\text{beat}}$  is the beat frequency between the laser and the comb components. The frequency of the laser ( $\nu_L$ ) is expressed as

$$\nu_L = n \times f_{\text{rep}} + f_{\text{beat}} + m \times f_{\text{CEO}}, \quad (1)$$

where  $n$  is a mode number of the comb component involved in the beat measurement,  $f_{\text{rep}}$  is repetition frequency of the combs, and  $m$  is an integer that is associated with the nonlinear processes:  $m = 2$  for the  $\chi^{(2)}$  process and  $m = 1$  for the  $\chi^{(3)}$  process. In the actual experiment, since the original comb is locked,  $f_{\text{rep}}$  and  $f_{\text{CEO}}$  have known values. When we measure  $f_{\text{beat}}$  using a frequency-stabilized laser with a known absolute frequency value, we should be able to determine both integers  $n$  and  $m$ . In this way, the nonlinear process that is involved in the spectral broadening can be determined by the absolute frequency measurement using the broadened comb.

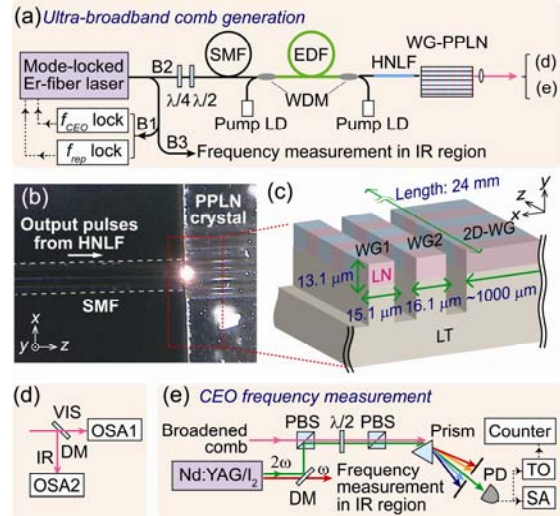


Fig. 2. (a) Experimental setup for an ultra-broadband comb generation. (b) Microscope image of the input-coupling to the PPLN-WG. (c) An illustration of the chip containing the PPLN-WGs on a lithium tantalate (LT) substrate. Setup for (d) measurements of the spectra, and (e) a frequency measurement of the broadened comb. B, branch;  $\lambda/4$ , quarter-wave plate;  $\lambda/2$ , half-wave plate; SMF, single-mode fiber; EDF, Er-doped fiber; WDM, wavelength division multiplexing; LD, laser diode; HNLF, highly-nonlinear fiber; PPLN-WG, periodically poled lithium niobate waveguide;  $f_{\text{CEO}}$ , carrier-envelope-offset frequency;  $f_{\text{rep}}$ , repetition-rate; 2D-WG, a quasi-parallel-plate waveguide; VIS, visible; IR, infrared; DM, dichroic mirror; OSA, optical spectrum analyzer; PBS, polarization beam splitter; PD, photodetector; SA, spectrum analyzer; TO, tracking oscillator.

### III. EXPERIMENTAL SETUP

Figure 2(a) shows a schematic of the experimental setup for an ultra-broadband comb generation. The output pulses from the mode-locked Er:fiber laser were divided into 3 branches. The first branch (B1) was used for the detection of  $f_{\text{rep}}$  and  $f_{\text{CEO}}$ , where  $f_{\text{rep}}$  and  $f_{\text{CEO}}$  were stabilized to a global positioning system disciplined oscillator (GPS-DO) time base. The second branch (B2) was used for wavelength conversion, where the light was amplified from 1.7 to 117 mW with an Er-doped fiber amplifier (EDFA) pumped both forward and backward by two laser diodes. Subsequently, the amplified pulse train was spectrally broadened in a highly nonlinear fiber (HNLF).

The output beam from the HNLF was then coupled into a PPLN-WG using butt coupling, as shown in Fig. 2(b). The dimensions of the PPLN-WG wafer (NTT Electronics Corporation, WD-3400-000-A-C-C) are  $24 \text{ mm} \times 0.5 \text{ mm} \times 6 \text{ mm}$  (length  $\times$  height  $\times$  width). Six waveguide groups (G1 to G6) were fabricated in the wafer, each with a different QPM grating period from  $28.50 \text{ }\mu\text{m}$  to  $28.75 \text{ }\mu\text{m}$  with a step of  $0.05 \text{ }\mu\text{m}$ . These QPM grating periods were designed for the DFG to convert NIR lights into a  $3\text{-}\mu\text{m}$  MIR light, as well as for the SHG of a  $2\text{-}\mu\text{m}$  fundamental light. Each group has two waveguides with the same height of  $13.1 \text{ }\mu\text{m}$  and different widths of  $16.1 \text{ }\mu\text{m}$  (WG1) and  $15.1 \text{ }\mu\text{m}$  (WG2). There is a buffer space between G3 and G4 with a width of  $1 \text{ mm}$  and a QPM grating period as the neighboring group [shown in Fig. 2(c)]. Therefore, the buffer space can be considered as a quasi-parallel-plate waveguide (2D-WG) with a waveguide structure only in the height direction (the direction of  $y$ ).

The input laser polarization of the PPLN-WG was linear and parallel to the  $y$ -axis. The throughput from the PPLN-WG was approximately 50%, and the estimated pulse energy was approximately  $0.5 \text{ nJ}$ , including the propagation loss and 14% Fresnel reflection at the output facet. The output pulses from the PPLN-WG were collimated by a lens and separated by a dichroic mirror into visible and IR light beams. As shown in Fig. 2(d), the spectrum of the visible and IR lights was observed using a grating optical spectrum analyzer (OSA1, 350 - 800 nm) and a Fourier-transform OSA (OSA2, 800 - 1700 nm), respectively.

We measured the CEO frequency of the broadened comb using an iodine-stabilized Nd:YAG laser (Nd:YAG/I<sub>2</sub>) at 532 nm. The Nd:YAG/I<sub>2</sub> was frequency-stabilized to a Doppler-free iodine signal of the  $a_{10}$  hyperfine component of the R(56)32-0 transition and has a known absolute frequency [17]. As shown in Fig. 2(e), the visible light of the Nd:YAG/I<sub>2</sub> was combined with the broadened comb by a polarization beam splitter (PBS), passed through a half-wave plate and another PBS, and then dispersed with a prism. The beat note between a comb mode and the Nd:YAG/I<sub>2</sub> were detected with a photo detector (PD). The detected signal was measured using an RF spectrum analyzer or a frequency counter through a

tracking oscillator. The frequency of the fundamental light of Nd:YAG/I<sub>2</sub> was also measured with the original Er:fiber comb provided by the third branch (B3).

### IV. RESULTS

#### A. Generation of ultra-broadband combs

Figure 3 shows the spectra of the observed ultra-broadband combs together with that of the original comb. The spectral sensitivity of OSA1 was not calibrated, and the spectra measured by OSA1 were rescaled to match OSA2 in the 800 nm region. The spectra of the output pulses from the laser cavity (thin green line), the EDFA (dot-dashed orange line) and the HNLF (dashed purple line) are also shown for comparison.

We observed a spectrum from 390 to 1000 nm, which was broadened from the original comb in G3-WG1 (the red curve in Fig. 3). There are several sharp peaks in the spectrum: (A)  $1.0 \text{ }\mu\text{m}$ , (B)  $690 \text{ nm}$ , (C)  $600 \text{ nm}$ , (D)  $550 \text{ nm}$ , and (E)  $506 \text{ nm}$ . Peak (A) is explained by phase-matching SHG from the  $2\text{-}\mu\text{m}$  fundamental light allowed by the first-order QPM grating period [18]. Other peaks are discussed in Section V. The visible part of the ultra-broadband comb was also confirmed by a spectrogram dispersed with a prism and taken with a digital camera, as shown in the inset of Fig. 3. The spectral distribution in the visible regime can be qualitatively compared with the result in [11], since similar PPLN-WGs were used in both experiments. We note that a MIR spectrum around  $3.5 \text{ }\mu\text{m}$  should also be generated based on the designed

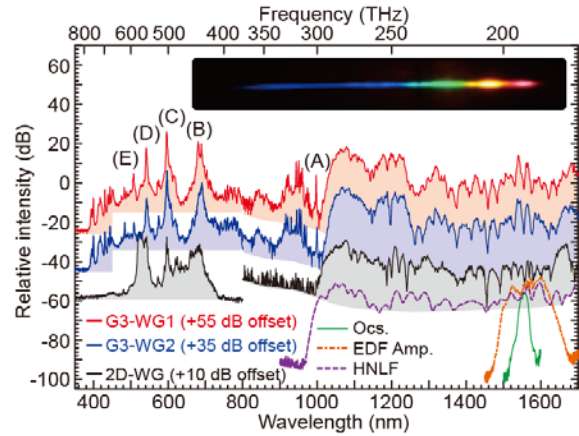


Fig. 3. Observed ultra-broadband comb spectra from 390 nm to 1700 nm in PPLN-WG with different widths. The bottoms of the shaded regions indicate the noise-floor of the OSA. (A)-(E) indicate sharp peaks at (A)  $1.0 \text{ }\mu\text{m}$ , (B)  $690 \text{ nm}$ , (C)  $600 \text{ nm}$ , (D)  $550 \text{ nm}$ , and (E)  $506 \text{ nm}$ , respectively. The spectra of the output pulse from the laser cavity (thin green line), EDFA (dot-dashed orange line), and the octave-spanning OFC from the HNLF (dashed purple line) are also shown. The inset indicates a spectrogram of the broadband comb in the visible region.

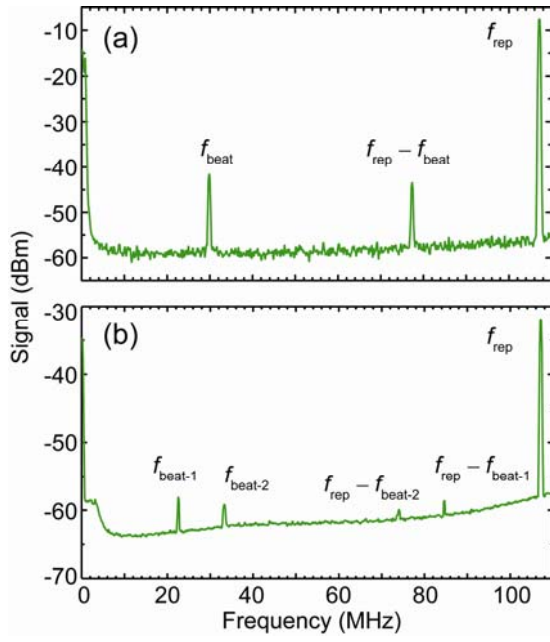


Fig. 4. Spectrum of beat signals between the frequency-doubled Nd:YAG laser and the optical frequency comb components at 532 nm.  $f_{\text{beat}}$  is the beat frequency between the laser and nearest comb mode,  $f_{\text{rep}}$  is the repetition rate of the comb, and  $(f_{\text{rep}} - f_{\text{beat}})$  is the beat frequency between the laser and second-nearest comb mode. (a) One pair of  $f_{\text{beat}}$  observed. The resolution bandwidth (RBW) is 300 kHz and the video bandwidth (VBW) is 10 kHz. (b) Two pairs of  $f_{\text{beat}}$  observed. The RBW is 300 kHz and the VBW is 300 Hz. Here, we slightly adjusted the polarization of the laser light by rotating the waveplates in front of the EDFA to maximize the  $f_{\text{beat-2}}$  signal.

phase-matching DFG but was not observed due to the long wavelength limit of OSA2. When the power level incident on the PPLN-WG was approximately 117 mW, the ultra-broadband comb in the visible region ( $< 700$  nm) provided approximately 29 mW on a thermal power meter. The simple ratio of the visible output power to the total incident power was approximately 25% and is quantitatively consistent with that in [11].

We also investigated the dependence of the spectrum on the width of the waveguide. The spectrum for G3-WG2 is shown in Fig. 3 with a blue curve, which is similar compared to that for G3-WG1. Hence, there is no significant dependence on a few percent variation of the waveguide width. As an example of a large variation of the waveguide width, we also show the spectrum emitted from the 2D-WG with a black line in Fig. 3. In this case, the peak intensity of the pulses in the waveguide decreases to a few tenths of that in a three-dimensional waveguide, as the input beam is confined only in the  $y$  direction but spatially spreads in the  $x$  direction with a divergence angle of the single-mode fiber before the

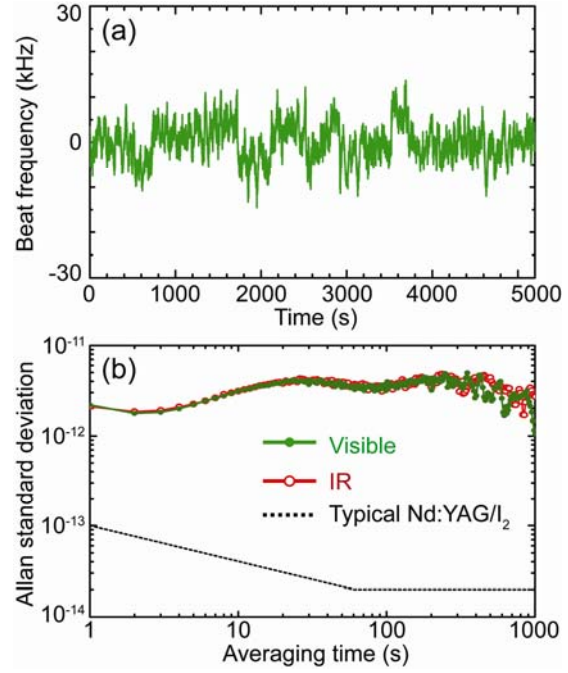


Fig. 5. (a) Temporal variation of the beat frequency between the broadened comb and the visible light of the Nd:YAG/I<sub>2</sub>. (b) Allan standard deviations of the beat frequencies. The red curve with open circles is for the measured beat frequency between the original comb and the fundamental light of the Nd:YAG/I<sub>2</sub>. The green curve with solid circles is for the measured beat frequency between the broadened comb and the visible light of the Nd:YAG/I<sub>2</sub>. For comparison, the Allan standard deviation of a typical Nd:YAG/I<sub>2</sub> (dotted curve) are shown.

waveguide. A broad spectrum spanning from 500 to 740 nm was generated, even for such a weak peak intensity. However, no spectrum was generated in the range of 740 - 1000 nm, or  $< 500$  nm.

## B. Measurement of CEO frequencies of the ultra-broadband comb

Figure 4(a) shows the observed beat signals between the Nd:YAG/I<sub>2</sub> and the broadened comb at 532 nm. The observed  $f_{\text{beat}}$  around 30 MHz has a signal-to-noise ratio (S/N) of approximately 20 dB at a resolution bandwidth (RBW) of 300 kHz. We measured  $f_{\text{beat}}$  using a frequency counter through a tracking oscillator for 5000 s with an average time ( $\tau$ ) of 1 s [shown in Fig. 5(a)]. The corresponding Allan standard deviation calculated from the measured  $f_{\text{beat}}$  is shown in Fig. 5(b) as green solid circles. The calculated Allan standard deviation was limited by the frequency stability of the GPS-DO because the stability of the Nd:YAG/I<sub>2</sub> [shown as a dotted curve in Fig. 5(b)] is much better. In the present experiment,  $f_{\text{rep}}$  and  $f_{\text{CEO}}$  were fixed at 107,007,267.7 Hz and  $-10,692,000$  Hz, respectively. Using the measured  $f_{\text{beat}}$  of



$-29,519.4 \text{ kHz} \pm 0.6 \text{ kHz}$  (uncertainty was obtained from the Allan standard deviation at  $\tau = 1000 \text{ s}$ ), we calculated  $\nu_L$ ,  $n$ , and  $m$  from Eq. (1).  $n$  was determined to be 5,263,757 using additional information of the known frequency value of the Nd:YAG/I<sub>2</sub> [17].  $\nu_L$  and  $m$  were calculated to be  $563,260,203,503.4 \text{ kHz} \pm 0.6 \text{ kHz}$  and 2, respectively. The result of  $m = 2$  reveals that the broadened comb was generated through the  $\chi^{(2)}$  process (Case I), as discussed in Section II.

$\nu_L$  can also be calculated from the measured beat frequency between the fundamental light of Nd:YAG/I<sub>2</sub> and the original comb. Using the data with a total measurement time of 5000 s, we obtained the absolute frequency of the fundamental light of the Nd:YAG/I<sub>2</sub> as  $281,630,101,752.23 \text{ kHz} \pm 0.78 \text{ kHz}$ . This resulted in an absolute frequency of a frequency-doubled light at 532 nm as  $563,260,203,504.5 \text{ kHz} \pm 1.6 \text{ kHz}$ , which agrees with the laser frequency measured using the broadened comb at 532 nm within the measurement uncertainties. We also show the Allan standard deviation determined from the measured beat frequency between the fundamental light of the Nd:YAG/I<sub>2</sub> and the original comb as red open circles in Fig. 5(b). The Allan standard deviations obtained using the original and broadened combs are in good agreement. Since the optical power of individual comb component is weak due to the broadening of the comb spectrum, the obtained relatively small S/N of the beat signals could affect the accuracy of absolute frequency measurements. Here, we have demonstrated and verified that a broadened comb is fully capable of absolute frequency measurements.

### C. Self-referenced CEO beat signals of the ultra-broadband comb

When the broadband comb generation involves several nonlinear processes, one can expect to observe a self-referenced CEO beat signal in some cases. The self-referenced CEO beat signal is observed directly from the PPLN-WGs without a separate interferometer or additional alignments. Self-referenced CEO beat signals were observed using PPLN-WGs at green and red wavelengths [11] and at 700 nm [10] using Er: fiber combs, and at 566 nm and 796 nm using a Tm: fiber comb [14]. The CEO beat signals can be generated based on the  $f - 2f$ ,  $2f - 3f$ , or  $3f - 4f$  interference between different comb series. In most cases, the process that generates the CEO beat signal was not self-evident.

Figure 6 shows the observed self-referenced CEO beat signals using our obtained ultra-broadband comb. We dispersed the broadened comb by a prism and spatially selected the comb modes at a certain wavelength using a slit. At each wavelength, we adjusted the polarization of the laser light by rotating the waveplates in front of the EDFA to maximize the CEO beat signal. Here, the wavelengths read by the OSA1, from 480 to 900 nm, have an uncertainty of a few nanometers. Interestingly, we were able to observe the CEO beat signal at 10.7 MHz across the whole broadened comb from 480 to 900 nm.

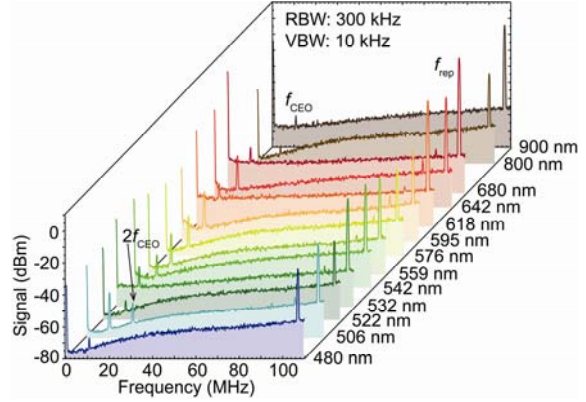


Fig. 6. The self-referenced CEO beat signals observed by detecting the comb components in the visible and IR wavelength regions. The resolution and video bandwidths of the RF spectrum analyzer were 300 kHz and 10 kHz, respectively.

We performed frequency measurements of the Nd:YAG/I<sub>2</sub> for the determination of the process that generates the CEO beat signals. When we changed the polarization of the laser light by rotating the waveplates in front of the EDFA for the optimization of the CEO beat signal, two pairs of beat signals could be observed between the Nd:YAG/I<sub>2</sub> and the broadened comb at 532 nm [shown in Fig. 4(b)]. This indicates that there were two broadened comb series in this case. Again, we tried to measure the CEO frequency of these two comb series.  $f_{\text{beat-1}}$  ( $f_{\text{beat-2}}$ ) had an S/N of approximately 5 dB (2 dB) and was not suitable for frequency measurement using a frequency counter. Therefore, we measured the frequency of  $f_{\text{beat-1}}$  and  $f_{\text{beat-2}}$  using the RF spectrum analyzer, which has an uncertainty of approximately 120 kHz. The frequency values of  $f_{\text{beat-1}}$  and  $f_{\text{beat-2}}$  were 22.52 MHz and 33.35 MHz, respectively.  $f_{\text{rep}}$  was fixed at 107,006,630.1 Hz.  $f_{\text{CEO}}$  and  $\nu_L$  were the same as the values in the previous measurements in this section. Using these values,  $m$  was determined to be 2 and 3 for the  $f_{\text{beat-1}}$  and  $f_{\text{beat-2}}$  comb series, respectively. This result reveals that the observed self-referenced CEO beat signal at 532 nm was generated based on the  $2f - 3f$  interference between the  $m = 2$  broadened comb and another  $m = 3$  comb series.

As discussed in Section II, we consider that the  $f_{\text{beat-2}}$  comb series with  $m = 3$  was generated by further SFG between the original comb and the  $f_{\text{beat-1}}$  comb series. We note that the spectral distribution of the broadened comb did not change drastically when we changed the polarization. Usually, the polarization change of the input light into the HNLF results in a significant change in the spectral distribution of the original comb after the HNLF. The SFG for the  $m = 3$  comb series at a certain wavelength can be enhanced or reduced due to the spectral variation in the original comb.

We consider that the observed self-referenced CEO beat signals from 480 to 900 nm are all based on the  $2f - 3f$  interference discussed above. However, further investigations

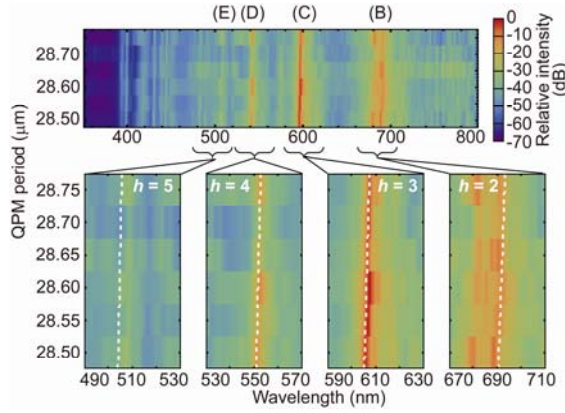


Fig. 7. Observed broadened comb spectra in WG1 as a function of the QPM period. The peaks of (B), (C), (D), and (E) are the same as those indicated in Fig. 3. The lower part shows the enlarged spectra near the peaks. The calculated results for the wavelengths of higher-order QPM SHG as a function of the QPM period are shown as dashed curves.

may be necessary to verify this. As shown in Fig. 6, we also observed a CEO beat signal with a frequency of  $2f_{\text{CEO}}$  when the wavelength was set at 506 nm. Peak (A) at 1.0  $\mu\text{m}$ , shown in Fig. 3, is explained as the first order QPM SHG of the original comb at 2.0  $\mu\text{m}$ . Therefore, some frequency components with a  $4f_{\text{CEO}}$  offset frequency could be generated at 0.5  $\mu\text{m}$  as a direct SHG from 1.0  $\mu\text{m}$ . These comb components could contribute to a  $2f - 4f$  interference for the observation of a  $2f_{\text{CEO}}$  beat signal.

## V. DISCUSSION AND CONCLUSION

In the present work, we use the frequency information of individual comb lines to determine the nonlinear process involved in the spectral broadening and the generation of self-referenced CEO beat signals. In contrast, previous works [13,14] have developed a numerical model [19,20] to describe the nonlinear interactions in QPM waveguides. This model accounts for the  $\chi^{(2)}$ , instantaneous  $\chi^{(3)}$ , and stimulated Raman scattering nonlinearities, including appropriate noise terms. Modal dispersion to all orders, nonlinear interactions between multiple waveguide modes, and multiple QPM orders are also included [21]. Using numerical simulations based on this model, it is understood that the main process for broadened comb generation is higher order QPM SHG due to the cascaded- $\chi^{(2)}$  process [13,14].

Here we report the observation of the spectral structure variation as a function of the QPM period, and discuss the observed variation using a calculation based on higher order QPM SHG. Figure 7 shows the observed broadened comb spectra in WG1 as a function of the QPM period. The enlarged spectra near the peaks of (B), (C), (D), and (E) are shown to be lower. Furthermore, the calculated results for the wavelengths of higher-order QPM SHG as a function of the QPM period

are represented by the dashed curves in Fig. 7. The SHG wavelengths were simply calculated using a phase matching condition of  $2\pi h/\Lambda = k_{2\omega} - 2k_{\omega}$ , where  $h$  is the order of Fourier component,  $\Lambda$  is the period of QPM, and  $\omega$  is the angular frequency of fundamental light. Here, the wavevector  $k_{\omega} = n(\omega)\omega/c$ , where  $c$  is the speed of light in vacuum and  $n(\omega)$  is the extraordinary refractive index of the lithium niobate waveguide for the fundamental mode. In the calculation of the  $n(\omega)$ , the Sellmeier equations and the coefficients reported in [22] were used. As shown in Fig. 7, the wavelengths of higher-order QPM SHG for  $h = 2, 3, 4$ , and  $5$  are quantitatively in good agreement with those of the observed peaks of (B), (C), (D), and (E), respectively. Furthermore, the observed spectral structure variation as a function of the QPM period could also be reproduced using our calculation. The obtained agreement of the observation and calculation related to the spectral variation caused by the change of the QPM period should provide important evidence to support the conclusion of higher order QPM SHG as a main process for ultra-broadband comb generation.

The clarification of the nonlinear processes involved in the generation of ultra-broadened combs is useful for the design and fabrication of nonlinear devices for such applications. For example, a frequency comb at a desired wavelength could be generated by using a PPLN-WG with a designed QPM period and order. A comb at a targeted wavelength may also be generated using further SFG between the original and broadened combs based on careful design of the nonlinear processes. For an Er:fiber comb, access to wavelengths at  $\lambda < 500$  nm is especially important as the generation of visible combs based on SHG with a bulk PPLN cannot reach these wavelengths. Other than the PPLN-WGs, a silicon nitride waveguide [23–25] and a silicon waveguide [26,27] should contribute to the ultra-broadband comb generation based on a chip-scale and fully-integrated device. Such new devices will eventually enable super broadband comb generation across terahertz, far-infrared, mid-infrared, near-infrared up to visible and ultraviolet [28,29].

In conclusion, we performed absolute frequency measurements using the ultra-broadband comb generated in a PPLN-WG. The measurement results directly reveal that the broadened comb is generated through the  $\chi^{(2)}$  process. We also determined that the self-referenced CEO beat signals observed in the ultra-broadband comb are based on the  $2f - 3f$  interference of different comb series. Furthermore, we experimentally and theoretically investigated spectral structure variation as a function of the QPM period. These results confirm that a main process for the ultra-broadband comb generation is higher order QPM SHG due to the cascaded- $\chi^{(2)}$  process. Our approach using optical frequency metrology is also applicable to investigations for nonlinear processes in other waveguides.

## ACKNOWLEDGMENTS

The authors would like to thank S. Okubo, H. Inaba, and Y. Nishida for their helpful discussions. This work was supported by the Japan Society for the Promotion of Science (JSPS) KAKENHI (15H02028, 18H01898, and 18H03886) and the Japan Science and Technology Agency (JST), Exploratory Research for Advanced Technology (ERATO) (JPMJER1304).

- [1] T. Udem, R. Holzwarth, and T. W. Hänsch, “Optical frequency metrology,” *Nature* **416**, 233–237 (2002).
- [2] F. L. Hong, “Optical frequency standards for time and length applications,” *Meas. Sci. Technol.* **28**(1), 012002 (2016).
- [3] T. Steinmetz, T. Wilken, C. Araujo-Hauck, R. Holzwarth, T. W. Hänsch, L. Pasquini, A. Manescau, S. D’Odorico, M. T. Murphy, T. Kentischer, W. Schmidt, and T. Udem, “Laser frequency combs for astronomical observations,” *Science* **321**, 1335–1337 (2008).
- [4] F. Adler, P. Masłowski, A. Foltynowicz, K. C. Cossel, T. C. Briles, I. Hartl, and J. Ye, “Mid-infrared Fourier transform spectroscopy with a broadband frequency comb,” *Opt. Express* **18**, 21861–21872 (2010).
- [5] D. J. Jones, S. A. Diddams, J. K. Ranka, A. Stentz, R. S. Windeler, J. L. Hall, and S. T. Cundiff, “Carrier-envelope phase control of femtosecond mode-locked lasers and direct optical frequency synthesis,” *Science* **288**, 635–639 (2000).
- [6] C. Erny, K. Moutzouris, J. Biegert, D. Kühlke, F. Adler, A. Leitenstorfer, and U. Keller, “Mid-infrared difference-frequency generation of ultrashort pulses tunable between 3.2 and 4.8  $\mu\text{m}$  from a compact fiber source,” *Opt. Lett.* **32**, 1138–1140 (2007).
- [7] A. Gambetta, N. Coluccelli, M. Cassinerio, D. Gatti, P. Laporta, G. Galzerano, and M. Marangoni, “Milliwatt-level frequency combs in the 8–14  $\mu\text{m}$  range via difference frequency generation from an Er:fiber oscillator,” *Opt. Lett.* **38**, 1155–1157 (2013).
- [8] N. Nishizawa, H. Mitsuzawa, J. Takayanagi, and K. Sumimura, “Generation of 0.45–1.38  $\mu\text{m}$  visible to near-infrared widely broadened supercontinuum using Er-doped ultrashort-pulse fiber laser system,” *J. Opt. Soc. Am. B* **26**, 426–430 (2009).
- [9] L. Huan, C. S. Ying, M. Fei, L. B. Ke, and F. Z. Jun, “Er-fiber femtosecond optical frequency comb covering visible light,” *Acta Phys. Sin.* **64**, 094204-1-7 (2015).
- [10] C. Langrock, M. M. Fejer, I. Hartl, and M. E. Fermann, “Generation of octave-spanning spectra inside reverse-proton-exchanged periodically poled lithium niobate waveguides,” *Opt. Lett.* **32**, 2478–2480 (2007).
- [11] K. Iwakuni, S. Okubo, O. Tadanaga, H. Inaba, A. Onae, F.-L. Hong, and H. Sasada, “Generation of a frequency comb spanning more than 3.6 octaves from ultraviolet to mid infrared,” *Opt. Lett.* **41**, 3980–3983 (2016).
- [12] G. Ycas, F. R. Giorgetta, E. Baumann, I. Coddington, D. Herman, S. A. Diddams, and N. R. Newbury, “High-coherence mid-infrared dual-comb spectroscopy spanning 2.6 to 5.2  $\mu\text{m}$ ,” *Nat. Photon.* **12**, 202–208 (2018).
- [13] A. S. Kowligy, A. Lind, D. D. Hickstein, D. R. Carlson, H. Timmers, N. Nader, F. C. Cruz, G. Ycas, S. B. Papp, and S. A. Diddams, “Mid-infrared frequency comb generation via cascaded quadratic nonlinearities in quasi-phase-matched waveguides,” *Opt. Lett.* **43**, 1678–1681 (2018).
- [14] C. R. Phillips, C. Langrock, J. S. Pelc, M. M. Fejer, J. Jiang, M. E. Fermann, and I. Hartl, “Supercontinuum generation in quasi-phase-matched LiNbO<sub>3</sub> waveguide pumped by a Tm-doped fiber laser system,” *Opt. Lett.* **36**, 3912–3914 (2011).
- [15] R. DeSalvo, D. J. Hagan, M. S. Bahae, G. Stegeman, E. W. V. Stryland, and H. Vanherzeele, “Self-focusing and self-defocusing by cascaded second-order effects in KTP,” *Opt. Lett.* **17**, 28–30 (1992).
- [16] D. D. Hickstein, H. Jung, D. R. Carlson, A. Lind, I. Coddington, K. Srinivasan, G. G. Ycas, D. C. Cole, A. Kowligy, C. Fredrick, S. Droste, E. S. Lamb, N. R. Newbury, H. X. Tang, S. A. Diddams, and S. B. Papp, “Ultrabroadband supercontinuum generation and frequency-comb stabilization using on-chip waveguides with both cubic and quadratic nonlinearities,” *Phys. Rev. Applied* **8**, 014025-1-8 (2017).
- [17] F.-L. Hong, J. Ishikawa, Y. Zhang, R. Guo, A. Onae, and H. Matsumoto, “Frequency reproducibility of an iodine-stabilized Nd:YAG laser at 532 nm,” *Opt. commun.* **235**, 377–385 (2004).
- [18] R. W. Boyd, *Nonlinear optics*, 3rd ed. (Elsevier, New York, 2008).
- [19] M. Conforti, F. Baronio, and C. De Angelis, “Nonlinear envelope equation for broadband optical pulses in quadratic media,” *Phys. Rev. A* **81**, 053841-1-4 (2010).
- [20] M. Conforti, F. Baronio, and C. De Angelis, “Ultrabroadband optical phenomena in quadratic nonlinear media,” *IEEE Photon. J.* **2**, 600–610 (2010).
- [21] C. R. Phillips, C. Langrock, J. S. Pelc, M. M. Fejer, I. Hartl, and M. E. Fermann, “Supercontinuum generation in quasi-phases-matched waveguides,” *Opt. Express* **19**, 18754–18773 (2011).
- [22] O. Tadanaga, T. Yanagawa, Y. Nishida, H. Miyazawa, K. Magari, M. Asobe, and H. Suzuki, “Widely tunable and highly efficient 2.3- $\mu\text{m}$ -band difference frequency generation in direct-bonded quasi-phase-matched LiNbO<sub>3</sub> ridge waveguide,” *Jpn. J. Appl. Phys.* **45**, L239–L241 (2006).
- [23] D. D. Hickstein, G. C. Kerber, D. R. Carlson, L. Chang, D. Westly, K. Srinivasan, A. Kowligy, J. E. Bowers, S. A. Diddams, and S. B. Papp, “Quasi-phase matched supercontinuum generation in photonic waveguides,”



- Phys. Rev. Lett. **120**, 053903-1-6 (2018).
- [24] A. Kowligy, D. D. Hickstein, A. Lind, D. R. Carlson, H. Timmers, N. Nader, D. L. Maser, D. Westly, K. Srinivasan, S. B. Papp, and S. A. Diddams, “Tunable mid-infrared generation via wide-band four-wave mixing in silicon nitride waveguides,” Opt. Lett. **43**, 4220–4223 (2018).
- [25] Y. Okawachi, M. Yu, J. Cardenas, X. Ji, A. Klenner, M. Lipson, and A. L. Gaeta, “Carrier envelope offset detection via simultaneous supercontinuum and second-harmonic generation in a silicon nitride waveguide,” Opt. Lett. **43**, 4627–4630 (2018).
- [26] N. Nader, D. L. Maser, F. C. Cruz, A. Kowligy, H. Timmers, J. Chiles, C. Fredrick, D. A. Westly, S. W. Nam, R. P. Mirin, J. M. Shainline, and S. A. Diddams, “Versatile silicon-waveguide supercontinuum for coherent mid-infrared spectroscopy,” APL Photonics **3**, 036102-1-10 (2018).
- [27] N. Singh, M. Xin, D. Vermeulen, K. Shtyrkova, N. Li, P. T. Callahan, E. S. Magden, A. Ruocco, N. Fahrenkopf, C. Baiocco, B. P.-P. Kuo, S. Radic, E. Ippen, F. Kärtner, and M. R. Watts, “Octave-spanning coherent supercontinuum generation in silicon on insulator from 1.06  $\mu\text{m}$  to beyond 2.4  $\mu\text{m}$ ,” Light: Sci. Appl. **7**, 17131-1-8 (2018).
- [28] A. S. Mayer, C. R. Phillips, C. Langrock, A. Klenner, A. R. Johnson, K. Luke, Y. Okawachi, M. Lipson, A. L. Gaeta, M. M. Fejer, and U. Keller, “Offset-free gigahertz midinfrared frequency comb based on optical parametric amplification in a periodically poled lithium niobate waveguide,” Phys. Rev. Applied **6**, 054009-1-10 (2016).
- [29] D. D. Hickstein, D. R. Carlson, A. Kowligy, M. Kirchner, S. R. Domingue, N. Nader, H. Timmers, A. Lind, G. G. Ycas, M. M. Murnane, H. C. Kapteyn, S. B. Papp, and S. A. Diddams, “High-harmonic generation in periodically poled waveguides,” Optica **4**, 1538–1544 (2017).